

Article

High-Order Engineering Fastest Controller and Its Application in Thermal Power Units

Shangyao Shi ¹, Jun Li ², Yijia Huo ³, Ruiqi Li ^{1,4} and Pengyun Chen ^{3,*} 

¹ School of Electrical and Control Engineering, North University of China, Taiyuan 030051, China; peter.shi@nuc.edu.cn (S.S.); 17835132399@163.com (R.L.)

² Electric Power Research Institute of Guangdong Power Grid Co., Ltd., Guangzhou 510080, China; lijun87388@163.com

³ School of Aerospace Engineering, North University of China, Taiyuan 030051, China; s202418007@st.nuc.edu.cn

⁴ School of Software Engineering, North University of China, Taiyuan 030051, China

* Correspondence: chenpengyun@nuc.edu.cn

Abstract: In the domain of industrial process control, the ubiquitous proportional–integral–derivative (PID) control paradigm, while foundational, is deemed insufficient amidst evolving complexities. In alignment with China’s strategic “dual-carbon” targets, extant thermal power installations are mandated to facilitate profound peak load navigation and expedited frequency modulation services. The incumbent PID control schema is found wanting in this regard, precipitating the imperative for an innovative process control technology to supplant the conventional PID regimen. Power system engineers have consequently devised the engineering fastest controller (EFC), which has adeptly succeeded PID control in nascent applications, thereby meeting the stringent control exigencies for deep peak regulation and agile frequency modulation. Employing rigorous theoretical analysis and sophisticated simulation experiments, this investigation meticulously compares the performance attributes of high-order controllers (HOCs) with the EFC. The empirical findings underscore the EFC’s pronounced superiority over PI, PID, and SOC in regulatory performance enhancements by 122.2%, 88.0%, and 77.3%, respectively, and in mitigating disturbances by 140.0%, 80.9%, and 54.5%, respectively. This study culminates in the assertion that the EFC represents a paradigmatic advancement in industrial control technology, not only manifesting pronounced performance benefits but also furnishing a robust theoretical scaffolding that transcends the performance zeniths of traditional PID and HOC technologies.

Keywords: industrial process control; noise power gain; proportional–integral–derivative controller; high-order controller; engineering fastest controller



Academic Editor: Jiaqiang E

Received: 5 December 2024

Revised: 16 January 2025

Accepted: 17 January 2025

Published: 20 January 2025

Citation: Shi, S.; Li, J.; Huo, Y.; Li, R.; Chen, P. High-Order Engineering Fastest Controller and Its Application in Thermal Power Units. *Energies* **2025**, *18*, 441. <https://doi.org/10.3390/en18020441>

Copyright: © 2025 by the authors. Licensee MDPI, Basel, Switzerland. This article is an open access article distributed under the terms and conditions of the Creative Commons Attribution (CC BY) license (<https://creativecommons.org/licenses/by/4.0/>).

1. Introduction

In the context of global carbon peaking and carbon neutrality [1], commonly referred to as the “double-carbon” energy target, new energy power sources such as wind power [2] and photovoltaic power [3] have been developed rapidly. However, one of the challenges associated with these new energy sources is their volatility and lack of regulation. As new energy power generation continues to be integrated into the power grid, the proportion of the amount the power grid facing the new power consumption pressure continuously increases. In order to effectively solve the “abandoned wind” [4], “abandoned light” [5] problem, the current stage of the grid urgently needs to rapidly increase the depth of

the peak and the fast frequency regulation capacity. Traditional coal-fired thermal power generating units [6], that is, thermal power units, are still the basic component of the power generation side. The objective requirements of the thermal power units in service are to provide deep peaking and fast frequency regulation services that are simple to understand. Sacrificing the traditional thermal power units of power generation to promote the rapid development of new energy power is the objective choice to accelerate the development of new energy power at this stage. However, significantly improving the depth of the existing thermal power units of peaking and fast frequency regulation performance is a relatively complex technical problem, representing a challenge for the technical personnel of power companies. Deep peaking and fast frequency regulation performance is a relatively complex technical issue that challenges the technical staff of power companies. From the control point of view, the existing thermal power unit process control based on PID [7,8] control is not enough to continue to meet the new energy power of large-scale grid-connected control needs, heralding in the new energy power behind the rapid development of the process control technology. The rapid development of the new energy power behind the process control technology produces new needs, and the objective need to replace the existing PID control, in essence, is a significant breakthrough in the existing PID control performance ceiling.

Huang et al. [9] emphasized that “control science itself belongs to technical science, and the primary driving force for its development should be the needs of national or human development”. In the power system, since 2016, in the power engineering practice, the technicians of power enterprises have identified a significant issue: traditional PID control. The role of the CI [10] used in traditional PID control is not efficient, which is to build the CI basis of the FOIF behind the exponential tracking filtering mechanism. The FOIF is the basis for the construction of the PID structure. Reference [11] pointed out that: “PID control represents an exponential control mechanism”, and the breakthrough of the existing PID control is essentially from the filtering point of view of the exponential tracking filtering mechanism behind the FOIF. Based on this understanding, the technicians of power grid enterprises invented an EFTF, which significantly improves the performance of the filter output tracking filter input, and an EFC, which represents a new industrial process control technology that significantly improves the feedback control performance relative to traditional PID control. The EFC, which represents a new industrial process control technology, is developed based on the EFTF and obviously improves the feedback control performance relative to traditional PID control.

As of 2022, the EFC has been implemented in various aspects of commercial technological reform projects such as auxiliary frequency control [11–14], control of the denitrification system [15], control of the steam temperature system [16], and other aspects of the existing thermal power units in a certain province. It has been realized to replace PID control in large-scale applications. Shi et al. [17] point out that “The auxiliary frequency regulation external control system developed with EFC as the core has been rapidly popularized in main thermal power units in Guangdong Province. During the period from January 2020 to June 2021, it has been applied to 3 thermal power units (with a total capacity of 25,600 MW) for auxiliary frequency regulation external control system commercial contract projects”. The aim of replacing PID control is not to overthrow the basic PID structure but to consider the EFC as a basic PI plus filter structure. At the present stage, the EFC plays an important role in promoting the large-scale consumption of new energy power in the power grid and ensuring the safe and stable operation of the power grid. In addition, Reference [17] introduced the EFC into advanced weapon control systems.

The EFC is an important technical advancement in engineering practice, with theoretical issues behind it. In the face of this emerging process control technology, i.e., the EFC,

research work has been initiated by research teams in power grids, including, in particular, some university teams. However, the structure of the EFC is not conducive to theoretical research. At the present stage, the research mainly analyzes the mathematical analysis from the perspective of the frequency domain method and gives the theoretical basis of the EFC beyond traditional PID control.

In order to avoid conflicts with the existing research, the contents of this paper primarily address topics that have not been discussed in the existing research.

In the case not specified in the text, the unit of time constant, time, etc., is s ; the unit of frequency ω is rad/s , gain, ratio, etc., is dimensionless natural numbers; the unit of phase margin, phase, etc., is degree ($^\circ$); the order is a dimensionless natural integer; the commonly used logarithmic 20 lg unit is dB; the numerical computation interval for the simulation experiments is 0.5 s; and the input of the process of the simulation experiments and the process of the process are given as units of steps.

2. Control Constraints in the Industrial Environment

In the industrial environment, there are various types of interferences. The interference discussed in this paper mainly includes two persistent types of interference that always exists. The first type is the interference caused by the external environment on thermal power units. For example, there are obvious stochastic interference components in the power signal, mainly caused by random fluctuations in the grid's electricity side of the load, including new energy power load random fluctuations caused by power signals directly used for important control system feedback. The second type is related to the system process of interference in thermal power units. For example, boiler combustion has obvious randomness, and process signals such as wind pressure, wind temperature, water level, steam pressure, steam temperature, and other process signals carry obvious random interference components. The amplitude of these random interferences are not the same; for example, wind pressure, water levels, and other process signals in the amplitude of the random interferences are relatively high and steam pressure, steam temperature, and other process signals in the amplitude of random interferences are relatively low. The amplitude of these random interferences varies from 0.2% to 30% of the range of the process signals, such as wind pressure, water level, and other process signals.

The effect of random disturbances has always been an important issue in control systems; however, there is a notable lack of comprehensive and in-depth research regarding their effects on control systems. Referring to Shannon's information theory [18], the SNR [19] is regarded as a constraint that directly determines the transmission rate and the quality of information, such as the bit error rate of digital information [20]. In power systems, the SNR of an industrial frequency signal directly affects the accuracy of power frequency measurements. While the SNR is also important for control systems, its direct impact on the performance of control systems is not clear, so how to assess the impact of SNR also lacks a unified standard. Reference [14] converted the SNR into an NPG problem and categorized the NPG as an aspect of the SNR. The NPG provides an intuitive constraint principle. The NPG is:

$$npg = \frac{\int_{-T_{npg}}^0 [n_{out}(t)]^2 dt}{\int_{-T_{npg}}^0 [n_{int}(t)]^2 dt} \quad (1)$$

where npg is the calculation result of the NPG; $n_{out}(t)$ is the output of noise disturbance; $n_{int}(t)$ is the input of noise disturbance; T_{npg} is the time of calculating npg ; and T_{npg} is 2000 s by default in this paper.

Most of the control processes in thermal power plants are characterized by higher order inertia [21], i.e., higher-order characteristics and higher-order hysteresis [22]. For

these processes, a large number of PI controls is used in reality because PI has only two parameters. In the use of simpler PID, PI belongs to the category of PID. In higher-order processes, PI control performance is limited; in order to improve the control performance, there is a need to use PID, including HOCs. In practice, it has been found that the improvement in HOC performance relative to PID is not significant, and there may be some unrecognized problems. One reason is that some industrial environments require that HOCs cannot amplify random disturbances. The HOLO is a basic component of HOCs, and the main problem of the HOLO is the amplification of random disturbances. Undifferentiated, the LO has the problem of the amplification of random disturbances, and the control constraints of industrial environments are not taken into account in the design of the LO. Another reason is that even under the control constraints of the industrial environment, the LO with different construction structures may have very different ahead-of-time performances.

In terms of the effects of random disturbances, the regulating mechanism of the process control loop in a thermal power unit mainly consists of the electric regulating mechanism and the pneumatic regulating mechanism. For electric regulators, the peak-to-peak value of random disturbances should not exceed 5% or more of the control signal travel. For pneumatic regulators, the peak-to-peak values of random disturbances should not exceed 10% of the control signal travel. This is because the peak-to-peak value of the random interference is too high to accelerate the damage of the regulating mechanism, such as causing motor coil overheating and burning, accelerating mechanical wear and tear, and even causing unplanned downtime for accidents, resulting in large economic losses while the planned downtime maintenance is normal.

Taking an LO as an example, a pseudo-random signal with zero mean and a variation range of ± 0.01 is input, and the obtained random interference output $n_{out}(t)$ results are shown in Figure 1.

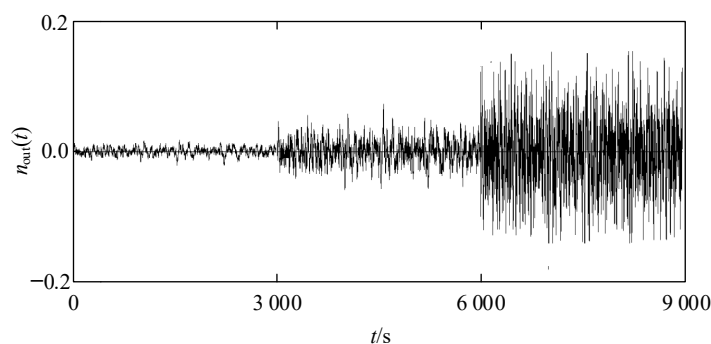


Figure 1. The random interference output results.

As shown in Figure 1, the average peak-to-peak value of random interference was 2.8% with t in the interval of 0 s–3000 s, $NPG = 1$, and the control signal traveling at 100%. With t in the 3000 s–5000 s interval and $NPG = 10$, the average peak-to-peak value of random disturbances was 8.9%. With t in the interval of 6000 s–9000 s and $NPG = 100$, the average peak-to-peak value of random interference was 28.3%. Only based on the qualitative judgment of the results given in Figure 1, for the electric regulator, the NPG should not be more than 1 and for the pneumatic regulator, the NPG should not be more than 10; however, this is not absolute. If process signals in the amplitude of the random interference are relatively small, $NPG = 100$ may meet the needs. On the other hand, if the amplitude of random interference in the process signal is high, $NPG = 1$ may not be sufficient.

The NPG represents a control constraint principle for industrial environments. In a general sense, an NPG value not greater than 10 belongs to a lower level of noise interference amplification, which is suitable for industrial environments. The significance of the NPG is also to provide a reference standard for the performance comparison of the LO with

two different build structures; however, the constraints discussed in this paper are not representative of the full range of constraints in the industrial environment.

3. Limitations of Higher-Order Controllers

Considering HOCs as a kind of series structure of PI and the HOLO, and PID as a kind of series structure consisting of PI and PD, PD represents the first-order over-observer.

There are two types of leading observers, referred to as the ATLO and BTLO, the difference being that the denominator of the ATLO is one order higher than the numerator, and the numerator of the denominator of the BTLO is of the same order. The ATLO and BTLO are

$$\begin{aligned} f_{\text{ATLO}}(s) &= \frac{(1 + \frac{T_{\text{LO}}}{n}s)^n}{(1 + \lambda \frac{T_{\text{LO}}}{n}s)^{n+1}}, \\ f_{\text{BTLO}}(s) &= \frac{(1 + \frac{T_{\text{LO}}}{n}s)^n}{(1 + \lambda \frac{T_{\text{LO}}}{n}s)^n}, \\ 0 < \lambda &\leq 1 \end{aligned} \quad (2)$$

where $f_{\text{ATLO}}(s)$ and $f_{\text{BTLO}}(s)$ are the transfer functions of the ATLO and BTLO, respectively; T_{LO} is the time constant of overrun, n is the order; and λ is the overrun coefficient.

3.1. Situational Analysis of the A-Type Over-the-Horizon Observer

Firstly, the performance of the ATLO was analyzed with respect to n . The experimental results obtained by setting $T_{\text{LO}} = 100$ s and $\text{NPG} = 10 \pm 0.5$ are shown in Table 1.

Table 1. Performance index of the ATLO.

Order/n	1	2	3	4
peak phase/°	54.8	68.9	72.0	72.3
peak gain/dB	20.17	21.93	21.93	21.64
λ	0.0491	0.177	0.301	0.401
Order/n	5	6	7	8
peak phase/°	71.9	70.9	69.7	68.7
peak gain/dB	21.36	20.96	20.56	20.26
λ	0.479	0.542	0.593	0.634

The peak phase value represents the ATLO's performance. Under the $\text{NPG} = 10$ constraint, the maximum performance of the ATLO is related to n . There exists an upper limit for n , and up to the upper limit, the performance of the ATLO is positively correlated with n . The peak phase value represents the maximum performance of the ATLO. Outside of the upper limit, the performance of the ATLO is inversely correlated with n .

At $n = 5$, the ATLO's frequency characteristics obtained are shown in Figure 2.

In Figure 2, $P_{\text{ATLO}}(\omega)$ is the phase–frequency phase of the ATLO and $G_{\text{ATLO}}(\omega)$ is the amplitude–frequency gain of the ATLO.

The ATLO is used to construct PID and SOC, and using λ given in Table 2, the PID and SOC values are obtained as

$$\begin{aligned} f_{\text{PI}}(s) &= K_P(1 + \frac{1}{T_I s}), \\ f_{\text{PID}}(s) &= f_{\text{PI}}(s) \frac{1 + T_{\text{LOS}}}{(1 + 0.0491 T_{\text{LOS}})^2}, \\ f_{\text{SOC}}(s) &= f_{\text{PI}}(s) \frac{(1 + \frac{T_{\text{LOS}}}{5}s)^5}{(1 + 0.479 \frac{T_{\text{LOS}}}{5}s)^6} \end{aligned} \quad (3)$$

where $f_{\text{PI}}(s)$, $f_{\text{PID}}(s)$, and $f_{\text{SOC}}(s)$ are the transfer functions of PI, PID, and SOC, respectively, and K_P and T_I are the proportional gain and integration constant of PI, respectively.

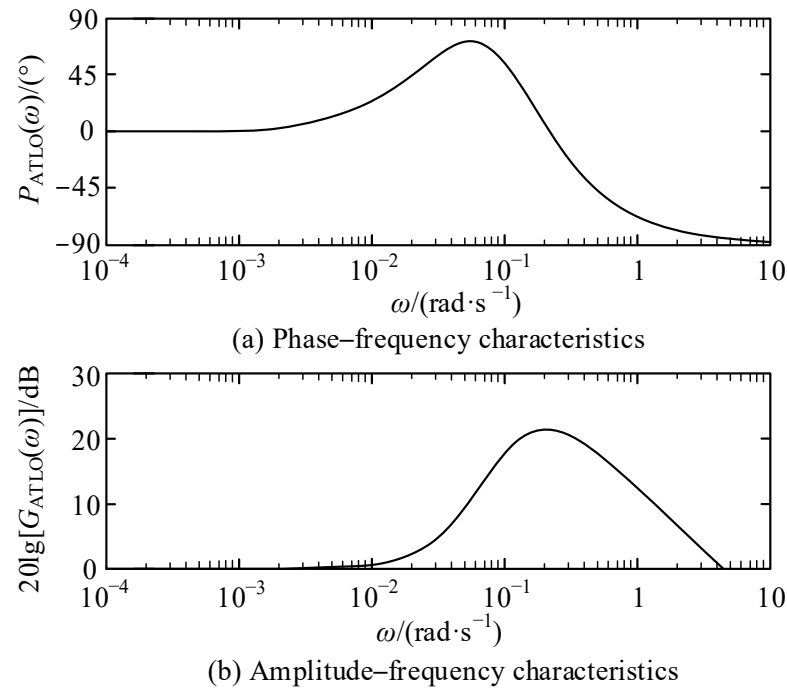


Figure 2. The frequency characteristics of the ATLO.

Table 2. Group A parameters of the controllers.

Controller	[TI:KP]min	KP	TI	
PI	105.96 s	1.039	110.1 s	
Controller	[TI:KP]min	KP	TI	TLO
PID	79.59 s	1.1057	88 s	75 s
Controller	[TI:KP]min	KP	TI	TLO
SOC	66.52 s	1.2327	82 s	197 s

The simulated control system was established and is shown in Figure 3.

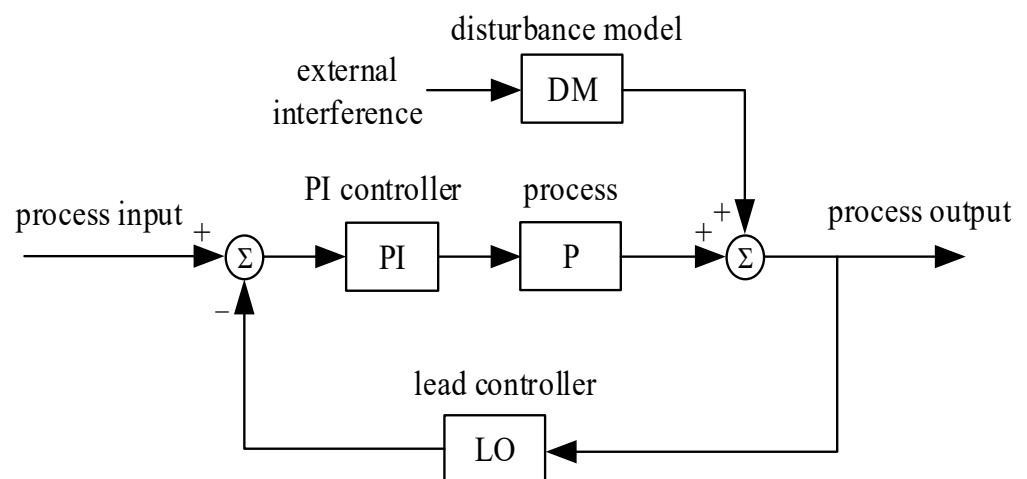


Figure 3. The simulation control system.

The external perturbation is directly coupled to the process output through the DM. Simply considered, the process of the DM is

$$\begin{aligned} f_P(s) &= \frac{P_G}{(1+T_P s)^6}, \\ f_{DM}(s) &= \frac{1}{(1+50s)^2}, \\ P_G &= 1, \\ T_P &= 50 \end{aligned} \quad (4)$$

where $f_P(s)$, P_G , and T_P are the transfer function of the process, the process gain, and the process time constant, respectively, and $f_{DM}(s)$ is the transfer function of the perturbation model.

After that, the default is $P_G = 1$ and $T_P = 50$ s, unless otherwise stated in the text.

The perturbation process of thermal power units typically exhibits the characteristics of an RF. Therefore, the use of an RF to measure the performance of the control system of external perturbation suppression has better intuition. In the RF perturbation stabilization of the process, the process output and the highest deviation from the set value were used to measure the performance of the external perturbation suppression. After that, the RF length was taken to be 2000 s and the RF rate was taken to be 10^{-3} s^{-1} , unless otherwise stated in the text.

The OLS of PI, PID, and SOC were

$$\begin{aligned} f_{PI:OLS}(s) &= f_{PI}(s)f_P(s), \\ f_{PID:OLS}(s) &= f_{PID}(s)f_P(s), \\ f_{SOC:OLS}(s) &= f_{SOC}(s)f_P(s) \end{aligned} \quad (5)$$

where $f_{PI:OLS}(s)$, $f_{PID:OLS}(s)$, and $f_{SOC:OLS}(s)$ are the transfer functions of the PI, PID, and SOC open-loop systems, respectively.

The open-loop system stability margin is:

$$\begin{aligned} F_{OLS}(j\omega) &= G_{OLS}(\omega)e^{P_{OLS}(\omega)}, \\ PM_{OLS} &= 180^\circ + P_{OLS}(\omega), \\ G_{OLS}(\omega)=1 \\ AM_{OLS} &= G_{OLS}(\omega) \\ P_{OLS}(\omega)=-180^\circ \end{aligned} \quad (6)$$

where $F_{OLS}(j\omega)$ is the frequency domain function of the open-loop system, $G_{OLS}(\omega)$ is the amplitude–frequency gain of the open-loop system; $P_{OLS}(\omega)$ is the phase–frequency phase of the open-loop system; PM_{OLS} is the phase margin of the open-loop system; and AM_{OLS} is the amplitude margin of the open-loop system.

At critical stabilization, $PM_{OLS} = 0^\circ$ and $AM_{OLS} = 0$ dB, and we searched for critical stabilization parameter ranges for PI, PID, and SOC. The curves of the relationship between $T_I : K_P$ and K_P for one group of PIs, and the curves of the relationship between $T_I : K_P$, K_P , and T_{LO} for multiple groups of PIDs and SOCs were obtained and are shown in Figure 4, Figure 5, and Figure 6, respectively.

The minimum value of $T_I : K_P$ is expressed in terms of $[T_I : K_P]_{\min}$, and the parameters corresponding to $T_I : K_P$ are selected from Figures 4–6, as shown in Table 2.

Group A controller parameters represent the highest control performance of PI, PID, and SOC under critical stabilization and are theoretically unique. RZFG is used to measure

the improvement in PID relative to PI control performance. The improvement in SOC relative to PI and PID control performance is

$$\begin{aligned} \lim_{s \rightarrow 0} \frac{f_{\text{PID:OLS}}(s)}{f_{\text{PI:OLS}}(s)} &\approx 1.331, \\ \lim_{s \rightarrow 0} \frac{f_{\text{SOC:OLS}}(s)}{f_{\text{PI:OLS}}(s)} &\approx 1.593, \\ \lim_{s \rightarrow 0} \frac{f_{\text{SOC:OLS}}(s)}{f_{\text{PID:OLS}}(s)} &\approx 1.197 \end{aligned} \tag{7}$$

Based on the results of Equation (7), the RZFG of PID is 1.331 times that of PI, the RZFG of SOC is 1.593 times that of PI, and the RZFG of SOC is 1.197 times that of PID. The results of the RZFG comparison represent a theoretical basis.

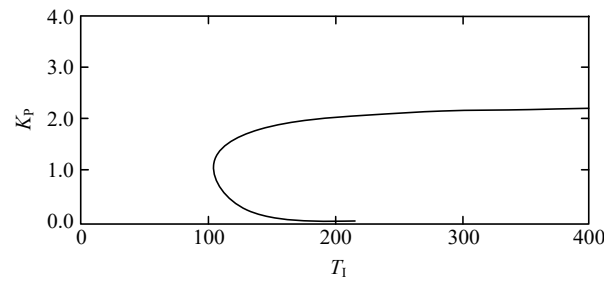


Figure 4. The search results of critical stability parameters of PI.

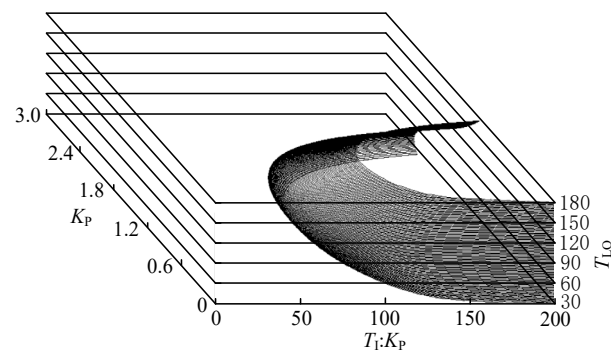


Figure 5. The search results of critical stability parameters of PID.

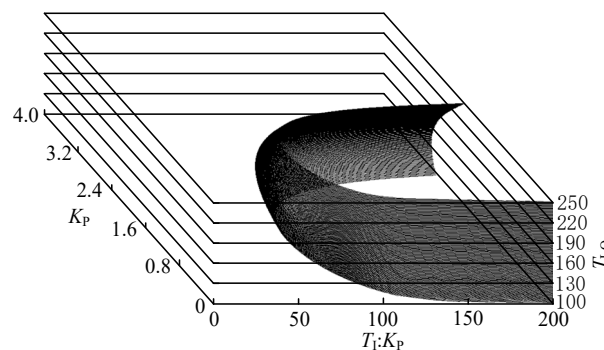


Figure 6. The search results of critical stability parameters of SOC.

Critical stability is not particularly meaningful for practical control systems. Reference [14] introduced the concept of the relative stability margin (RSM) but did not provide

a clear definition of the formula. Based on the supplementary information from Reference [14], the RSM was

$$\begin{aligned}
 RPM_{OLS} &= 180^\circ + P_{OLS}(\omega), \\
 20\lg[G_{OLS}(\omega)] &= G_{RV} \\
 RAM_{OLS} &= 20\lg[G_{OLS}(\omega)] \\
 P_{OLS}(\omega) &= -180^\circ + P_{RV}
 \end{aligned}
 \tag{8}$$

where RPM_{OLS} is the relative phase margin; G_{RV} is the relative value of magnitude margin; RAM_{OLS} is the relative magnitude margin; and P_{RV} is the relative value of phase margin.

Graphical representations of G_{RV} and P_{RV} are shown in Figure 7.

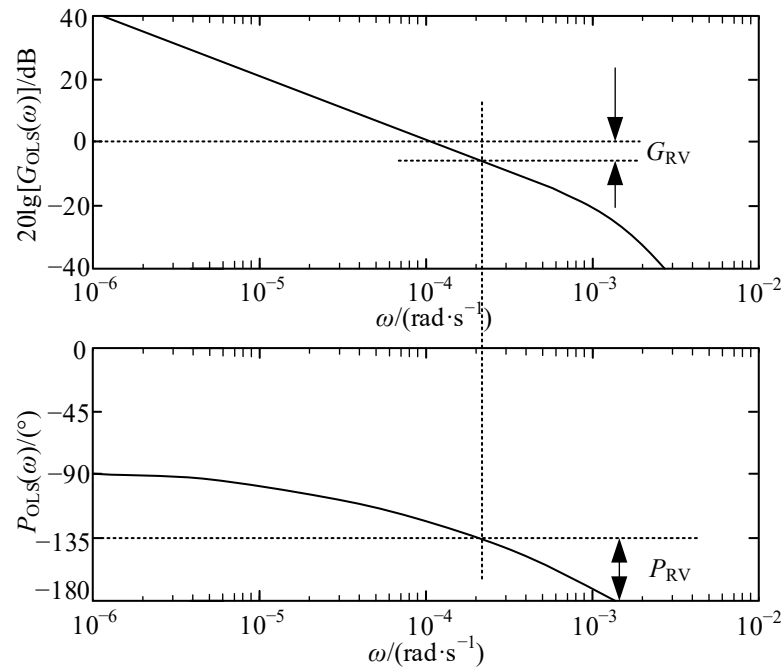


Figure 7. The relative stability margin.

Reference [14] suggested $G_{RV} = -6$ dB and $P_{RV} = 45^\circ$ with good robust performance, as shown in Figure 7.

According to the conditions of $G_{RV} = -6$ dB, $P_{RV} = 45^\circ$ was used to search for the PI, PID, and SOC parameters. For PID and SOC, the extracted $[T_I : K_P]_{min}$ corresponds to a set of $T_I : K_P, K_P$ between the change in the relationship between the curves. The obtained results of the parameter search are shown in Figure 8.

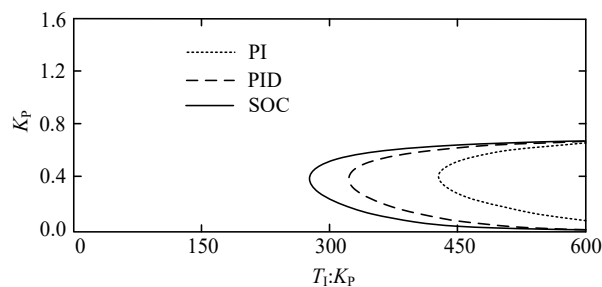


Figure 8. The parameter search results for PI, PID, and SOC.

Based on Figure 8, the PI, PID, and SOC parameters were obtained and are shown in Table 3.

Table 3. Group B parameters of the controllers.

Controller	[TI:KP]min	KP	TI	
PI [17]	428.42 s	0.4201	180 s	
Controller	[TI:KP]min	KP	TI	TLO
PID	321.76 s	0.3854	124 s	101 s
Controller	[TI:KP]min	KP	TI	TLO
SOC	274.69 s	0.3859	106 s	269 s

Based on the controller parameters of group B, the simulation experimental comparison results obtained are shown in Figure 9.

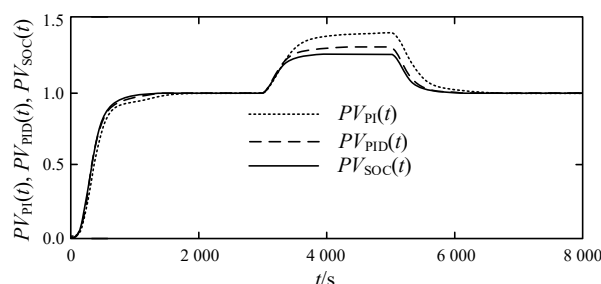


Figure 9. Comparison of the simulation experimental results of PI, PID, and SOC.

In Figure 9, $PV_{PI}(t)$, $PV_{PID}(t)$, and $PV_{SOC}(t)$ represent the process outputs of PI, PID, and SOC control, respectively.

Based on Figure 9, the performance indexes of PI, PID, and SOC control are compared in Table 4.

Table 4. Performance index of control of PI, PID, and SOC.

Control Methods	Peak 1	Peak 2	Process Overshoot	Adjustment Time/s
PI	1.0	1.0	0	1020
PID	1.0	1.0	0	863 s
SOC	1.0	1.0	0	814 s

In engineering, the regulation time is usually defined as the time in which the deviation in the process output from a given process value becomes less than 5%.

According to Table 5, the regulation performance of PID is improved by 18.2% with respect to PI. The regulation performance of SOC is improved by 25.3% with respect to PI and 6.0% with respect to PID.

Table 5. Performance index of disturbance rejection of PI, PID, and SOC.

Control Methods	Maximum Deviation During RF
PI	0.427
PID	0.322
SOC	0.275

Based on Figure 9, the performance indexes of PI, PID, and SOC external disturbance suppression are compared in Table 5.

According to Table 6, the perturbation rejection performance of PID is improved by 32.6% compared to PI. SOC's perturbation rejection performance is 55.3% higher than that of PI and 17.1% higher than that of PID.

Table 6. Performance index of the BTLO.

Order/n	1	2	3	4
peak phase/°	31.5	33.0	33.4	33.6
peak gain/dB	10.08	10.13	10.20	10.21
λ	0.313	0.558	0.676	0.745
Order/n	5	6	7	8
peak phase/°	33.7	34.1	34.2	34.3
peak gain/dB	10.23	10.34	10.38	10.39
λ	0.790	0.820	0.843	0.861

Compared with PI and PID, SOC control performance shows significant improvement. However, for some applications, such as FGBC for the reheat steam temperature in thermal power units, the enhancement in SOC control performance relative to PI and PID is not sufficient.

3.2. Situational Analysis of the B-Type Over-the-Horizon Observer

For the BTLO, the experimental results obtained by setting $T_{LO} = 100$ s and $NPG = 10 \pm 0.5$ are shown in Table 6.

Under the $NPG = 10$ constraint, the phase peak of the BTLO is low, and the BTLO does not perform well relative to the ATLO. The obvious problem with the BTLO is that it has no transcendence effect under the $NPG = 1$ constraint, i.e., $\lambda = 1$.

At $n = 5$, the obtained frequency characteristics of the BTLO are shown in Figure 10.

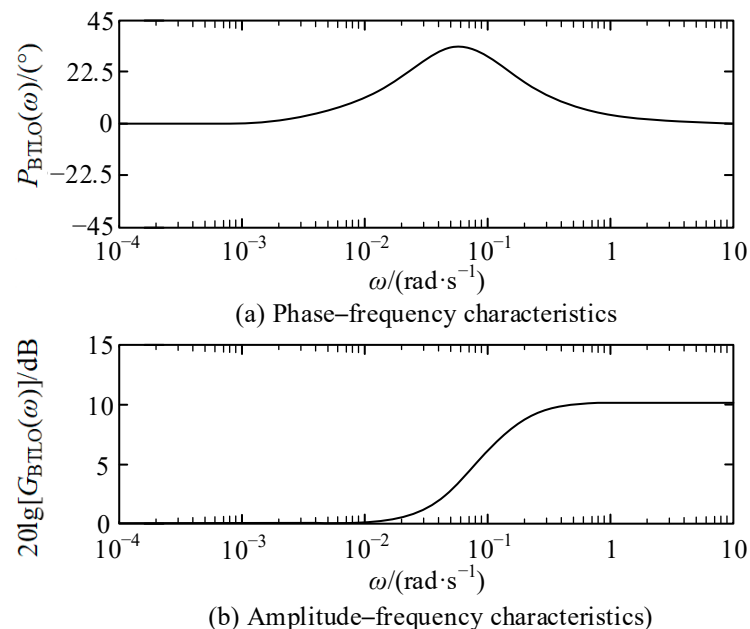


Figure 10. The frequency characteristics of the BTLO.

In Figure 10, $P_{BTLO}(\omega)$ is the phase frequency–phase of the BTLO, and $G_{BTLO}(\omega)$ is the amplitude–frequency gain of the BTLO.

The BTLO is used to construct the PID and SOC values, and for the sake of differentiation, PID and SOC are shown as lowercase PID and SOC. Using the λ given in Table 7, the PID and SOC values are

$$\begin{aligned} f_{pid}(s) &= f_{PI}(s) \frac{1+T_{LO}s}{1+0.313T_{LO}s}, \\ f_{soc}(s) &= f_{PI}(s) \frac{(1+\frac{T_{LO}s}{5})^5}{(1+0.790\frac{T_{LO}s}{5})^5} \end{aligned} \tag{9}$$

where $f_{pid}(s)$ and $f_{soc}(s)$ are the transfer functions of PID and SOC, respectively.

Table 7. Group C parameters of the controllers.

Controller	[TI:KP]min	KP	TI	TLO
PID	355.09 s	0.3858	137 s	96 s
Controller	[TI:KP]min	KP	TI	TLO
SOC	348.23 s	0.3848	134 s	327 s

For PID and SOC, the analysis of the critical stabilization parameters was not carried out, and the parameters of PID and SOC were searched only according to the principle of $G_{RV} = -6$ dB and $P_{RV} = 45^\circ$. Only a set of curves for the relationship between the changes in $T_I : K_P$ and K_P corresponding to $[T_I : K_P]_{min}$ were extracted, and the obtained results of the parameter search are shown in Figure 11.

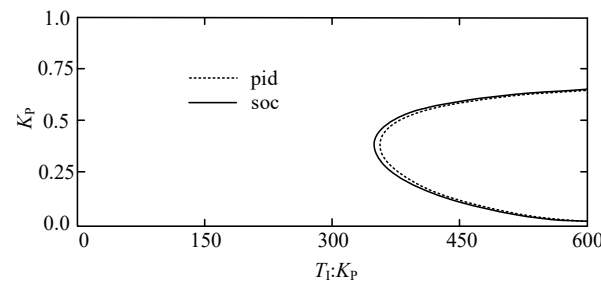


Figure 11. The parameter search results of PID and SOC.

Based on Figure 11, the PID and SOC parameters were obtained, as shown in Table 7.

According to the parameters of the group C controller, the simulation experimental comparison results of PID and SOC were obtained and compared with PI at the same time. The results are shown in Figure 12.

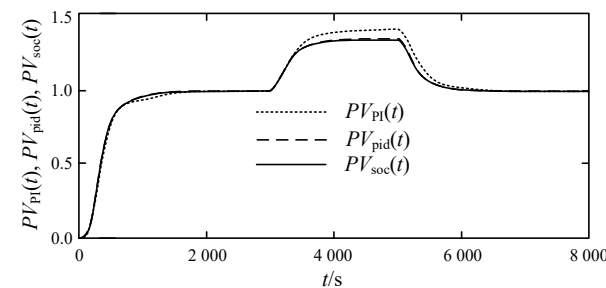


Figure 12. Comparison of the simulation experiments for PI, PID, and SOC.

In Figure 12, $PV_{pid}(t)$ and $PV_{soc}(t)$ represent the process output of PID and SOC control, respectively.

Based on Figure 12, the performance indexes of PID and SOC control were compared with PI, and the results are shown in Table 8.

Table 8. Performance index of the control of PI, PID, and SOC.

Control Methods	Peak 1	Peak 2	Process Overshoot	Adjustment Time/s
PI [17]	1.0	1.0	0	1020
PID	1.0	1.0	0	960 s
SOC	1.0	1.0	0	939 s

According to Table 8, the regulation performance of PID is improved by 6.3% with respect to PI. The regulation performance of SOC is improved by 8.6% with respect to PI and 2.2% with respect to PID.

Based on Figure 12, the performance indexes of PID and SOC external disturbance suppression were compared with PI, and the results are shown in Table 9.

Table 9. Performance index of the disturbance rejection of PI, PID, and SOC.

Control Methods	Maximum Deviation During RF
PI	0.427
PID	0.355
SOC	0.348

According to Table 9, the perturbation rejection performance of PID is improved by 20.3% with respect to PI. The perturbation rejection performance of SOC is 22.7% higher than that of PI and 2.0% higher than that of PID.

Compared with PID and SOC, the out-of-phase rejection performance of PID and SOC decreases significantly.

Under the constraint of $NPG = 10$, there is little difference between SOC and PID.

4. Engineering Maximum Speed Controller

The EFC is a cascade of EFPI controllers and the EFLO; the category of the EFC includes the AEFPI controller. The existing research mainly gives the theoretical basis and experimental results for the EFC and AEFPI. The theoretical basis that the EFC and AEFPI can significantly improve the performance of feedback control is given in References [14] and [17], respectively.

The EFC can also be a cascade of AEFPI and EFLO, for which no theoretical basis or experimental results have been given in the existing research. In order to fill the gap in the existing research, this paper mainly focuses on the research and experiments concerning the EFC of the AEFPI and EFLO tandem structure.

AEFPI is constructed based on AEFTE, and EFLO is constructed based on EFTF. AEFTE is an engineered reconstruction of AFTF, and EFTF is an engineered reconstruction of FTF.

4.1. Engineering Most Velocity Overrun Observer

EFLO represents a high-performance over-the-horizon observer and is essentially an inverse model of EFTF [23]. The physical defect of AFTF and FTF is the inclusion of pure hysteresis [24], so the inverse model of AFTF and FTF is not physically valid.

It has been pointed out before that “FOIF is the basis for the construction of PID structure”, and for the sake of comparison, FOIF, AEFTF, and EFTF are:

$$\begin{aligned}
 f_{FOIF}(s) &= \frac{1}{1 + T_{FOIF}s}, \\
 f_{AEFTF}(s) &= \frac{1}{16} \sum_{i=1}^{16} i \left(\frac{1}{1 + \frac{T_{AEFTF}}{16}s} \right)^i, \\
 f_{EFTF}(s) &= \frac{1}{16} \sum_{i=1}^{16} \left(\frac{1}{1 + \frac{T_{EFTF}}{16}s} \right)^i
 \end{aligned}
 \tag{10}$$

where $f_{FOIF}(s)$, $f_{AEFTF}(s)$, and $f_{EFTF}(s)$ are the transfer functions of FOIF, AEFTF, and EFTF, respectively, and T_{FOIF} , T_{AEFTF} , and T_{EFTF} are the time constants of FOIF, AEFTF, and EFTF, respectively.

At $T_{FOIF} = T_{AEFTF} = T_{EFTF} = 100$ s, the process outputs $PV_{FOIF}(t)$, $PV_{AEFTF}(t)$, and $PV_{EFTF}(t)$ for FOIF, AEFTF, and EFTF, respectively, were obtained, as shown in Figure 13.

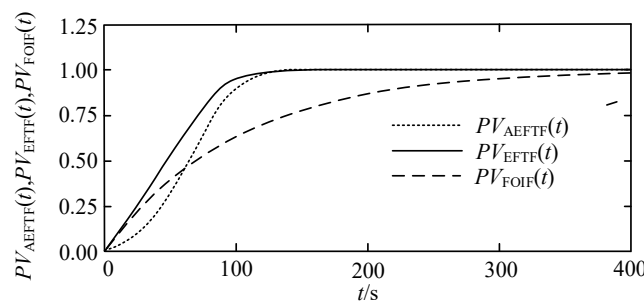


Figure 13. The process output of FOIF, AEFTF, and EFTF.

Compared with FOIF, AEFTF and EFTF significantly improve the performance of filter output tracking filter input, and AEFTF and EFTF break through the exponential tracking filter mechanism behind FOIF.

For comparison, FOIF was used to construct PI and AEFTF was used to construct AEFPI, and PI and AEFPI were obtained as:

$$\begin{aligned}
 f_{PI}(s) &= K_P \frac{1}{1 - f_{FOIF}(s)}, \\
 f_{AEFPI}(s) &= K_{AEFPI} \frac{1}{1 - f_{AEFTF}(s)}
 \end{aligned}
 \tag{11}$$

where $f_{AEFPI}(s)$ and K_{AEFPI} are the transfer function and proportional gain of AEFPI, respectively.

EFTF was used to construct EFLO, and EFLO was

$$\begin{aligned}
 f_{EFLO}(s) &= \frac{1.005}{0.005 + f_{EFTF}(s)} f_{SOF}(s), \\
 f_{SOF}(s) &= \frac{1}{(1 + T_{SOF}s)^2}
 \end{aligned}
 \tag{12}$$

where $f_{EFLO}(s)$ is the transfer function of EFLO, and $f_{SOF}(s)$ and T_{SOF} are the transfer function and time constant of SOF [25], respectively.

For comparison, the EFLO frequency characteristics were obtained by setting $T_{EFTF} = 100$ s, where in $T_{SOF} = 4.95$ s and $NPG = 10$, as shown in Figure 14.

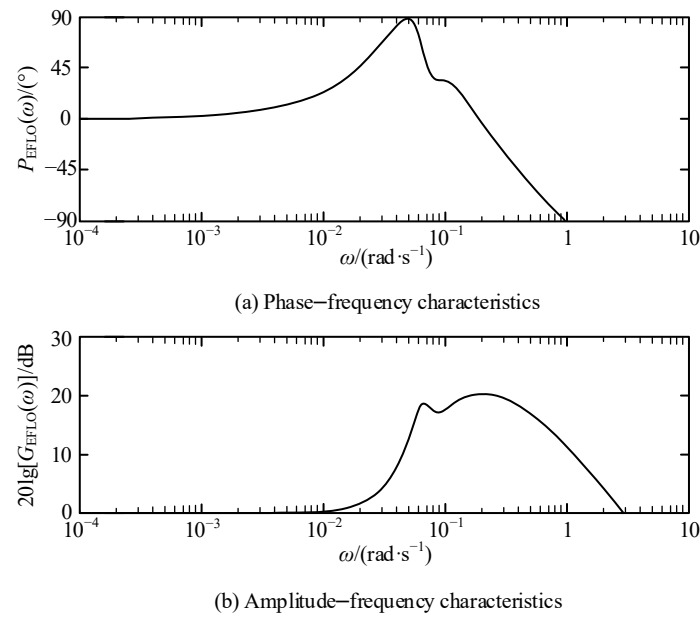


Figure 14. The frequency characteristic of EFLO.

In Figure 14, $P_{EFLO}(\omega)$ is the phase–frequency phase of EFLO, and $G_{EFLO}(\omega)$ is the amplitude–frequency gain of EFLO.

Based on Figure 14, the phase peak of EFLO is 88.3° and the gain peak is 20.8 dB, after which the default $T_{SOF} = 0.0495 T_{EFTF}$.

4.2. Open-Loop System Analysis

The EFC open-loop system is

$$\begin{aligned} f_{EFC:OLS}(s) &= f_{EFC}(s)f_P(s), \\ f_{EFC}(s) &= f_{AEFPI}(s)f_{EFLO}(s) \end{aligned} \tag{13}$$

where $f_{EFC:OLS}(s)$ is the transfer function of the EFC open-loop system and $f_{EFC}(s)$ is the transfer function of the EFC.

In the critical stabilization, the EFC critical stabilization parameters were searched, and the curves of the relationship between the changes in multiple $T_{AEFTF} : K_{AEFPI}, K_{AEFPI}$, and T_{EFTF} were obtained, as shown in Figure 15.

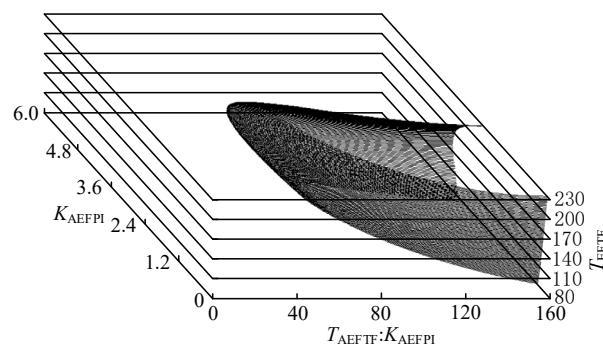


Figure 15. The search results of the critical stability parameters of the EFC.

Based on Figure 15, the critical stabilization parameters of the EFC were obtained, as shown in Table 10.

Table 10. Critical stability parameters of the EFC.

Controller	[TAEFTF:KAEFPI]min	KAEFPI	TAEFTF	TEFTF
EFC	57.42 s	3.9012	224 s	186 s

For comparison, RZFG was used to measure the improvement in the EFC relative to the upper limit of PI, PID, and SOC control performance. Based on Tables 3 and 10, the RZFG comparison results were obtained as follows

$$\begin{aligned}
 \lim_{s \rightarrow 0} \frac{f_{EFC:OLS}(s)}{f_{PI:OLS}(s)} &\approx 2.684, \\
 \lim_{s \rightarrow 0} \frac{f_{EFC:OLS}(s)}{f_{PID:OLS}(s)} &\approx 2.016, \\
 \lim_{s \rightarrow 0} \frac{f_{EFC:OLS}(s)}{f_{SOC:OLS}(s)} &\approx 1.685
 \end{aligned}
 \tag{14}$$

According to the results of Equation (14), the RZFG of the EFC is 2.684 times that of PI, 2.016 times that of PID, and 1.685 times that of SOC, which indicates that theoretically, the EFC significantly breaks through the upper limit of the control performance of PI, PID, and SOC.

4.3. Closed-Loop System Analysis

According to the conditions of $G_{RV} = -6$ dB, $P_{RV} = 45^\circ$ was used to search for the EFC parameters. We only extracted $[T_{AEFTF} : K_{AEFPI}]_{min}$ corresponding to a set of $T_{AEFTF} : K_{AEFPI}$, K_{AEFPI} change relationship curves between the obtained parameter search results, as shown in Figure 16.

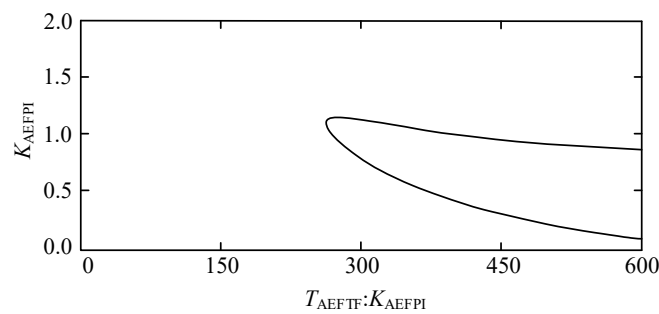


Figure 16. The search results of the parameters of the EFC.

Based on Figure 16, the EFC stabilization parameters were obtained and are shown in Table 11.

Table 11. Stability parameters of the EFC.

Controller	[TAEFTF:KAEFPI]min	KAEFPI	TAEFTF	TEFTF
EFC	263.38 s	1.090	287 s	239 s

According to the EFC parameters given in Table 11, the EFC was compared with PI, PID, and SOC, as shown in Figure 17.

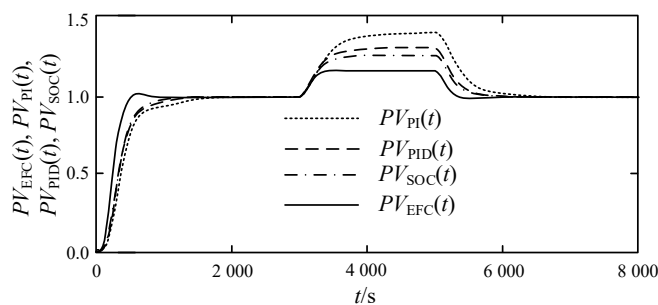


Figure 17. Comparison of the simulation experiments for the EFC and PI, PID, and SOC.

In Figure 17, $PV_{EFC}(t)$ represents the process output of EFC control.

Based on Figure 17, the performance indexes of EFC control were compared with PI, PID, and SOC, as shown in Table 12.

Table 12. Performance index of control of the EFC.

Control Methods	Peak 1	Peak 2	Process Overshoot	Adjustment Time/s
EFC	1.026	1.0	0.026	459 s
PI [17]	1.0	1.0	0	1020
PID	1.0	1.0	0	863 s
SOC	1.0	1.0	0	814 s

According to Table 12, the regulation performance of the EFC improved by 122.2% compared to PI, 88.0% with respect to PID, and 77.3% with respect to SOC.

Based on Figure 17, the performance indices of EFC external disturbance suppression were compared with PI, PID, and SOC, as shown in Table 13.

Table 13. Performance index of the disturbance rejection of the EFC.

Control Methods	Maximum Deviation During RF
EFC	0.178
PI	0.427
PID	0.322
SOC	0.275

According to Table 13, the EFC improves the perturbation rejection performance by 140.0% with respect to PI, 80.9% with respect to PID, and 54.5% with respect to SOC.

Compared with PI, PID, and SOC, the EFC control performance is significantly improved.

4.4. Robustness Analysis

The phase margin PM_{OLS} and amplitude margin AM_{OLS} of the open-loop system determine the stability of the closed-loop system, and the stability also needs to take into account the effects of the process P_G and T_P variations. Based on the EFC stabilization parameters given in Table 10, the relationship of PM_{OLS} with the variation in P_G and T_P is obtained, representing one aspect of the robustness analysis, as shown in Figure 18.

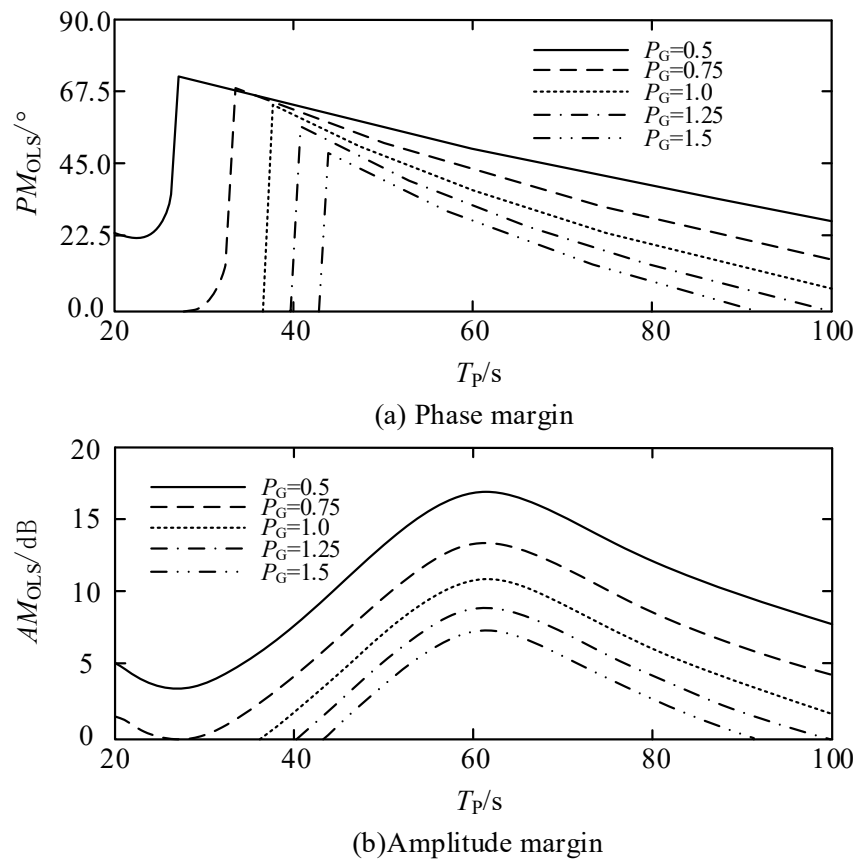


Figure 18. The result of the margin analysis is 1.

The problem cannot be overlooked. According to the stability margin analysis results presented in Figure 18, the robustness of the EFC is not good. One reason is that the EFC stabilization parameters given in Table 10 only represent the highest control performance at $G_{RV} = -6$ dB and $P_{RV} = 45^\circ$ and do not represent the robustness optimization.

The researchers identified a fundamental problem that the robustness of the EFC primarily depends mainly on the T_{TEFT} setting, which, in principle, is $T_{TEFT} \leq$ the inverse of the process frequency bandwidth, as follows

$$T_{TEFT} \leq \frac{1}{\omega_{PFB}} \tag{15}$$

where ω_{PFB} is the process frequency bandwidth.

For the given process, theoretically, $\omega_{PFB} = 0.006976$ rad/s; then, $T_{TEFT} \leq 143$. It is obvious that $T_{TEFT} > 143$ s given Table 10.

For comparison, based on the EFC stabilization parameters given in Table 10, by only changing $T_{TEFT} = 143$ s, the relationship of PM_{OLS} with the variation in P_G and T_P was obtained, as shown in Figure 19.

Figure 19 shows that changing only $T_{TEFT} = 143$ s significantly improves the robustness of the EFC with respect to the results of the stability margin analysis given in Figure 18.

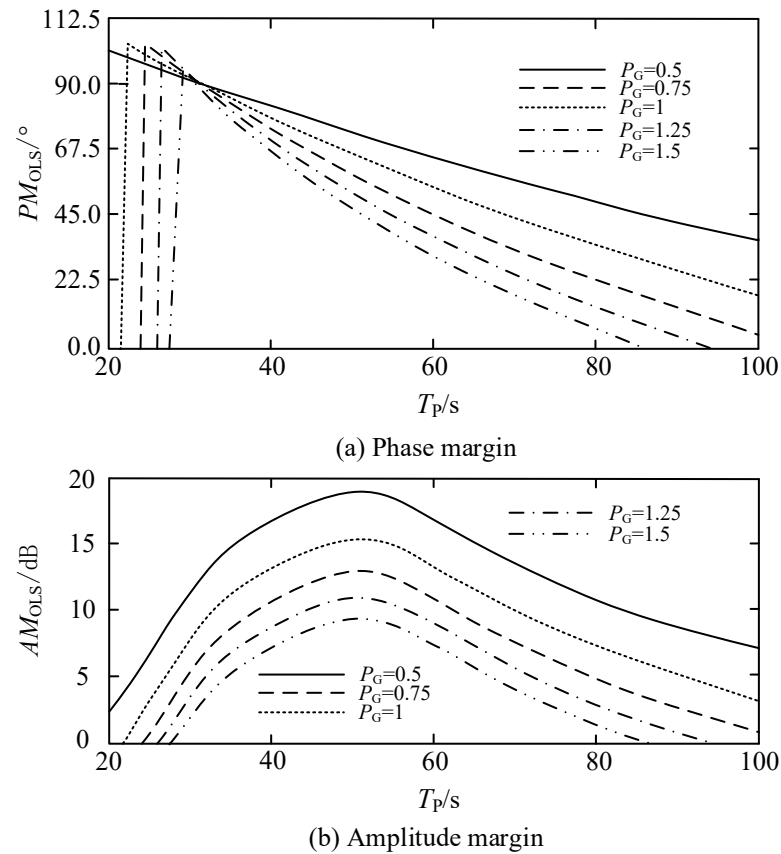


Figure 19. The result of the margin analysis is 2.

5. Engineering Parameterization of the Engineering Maximum Speed Controller

Controller parameterization is always an important issue, and the previous parameterization was based on the mathematical optimization method, which is based on a mathematical model. In engineering practice, obtaining accurate mathematical models can be challenging, making it difficult to depend on accurate mathematical models for parameter tuning.

Reference [17] presents the engineering tuning method for AEFPI parameters, and Reference [14] outlines the engineering tuning method for the EFC parameters for EFPI and EFLO structures. For the AEFPI and EFLO structures of the EFC, the parameterization method is as follows

$$\begin{aligned}
 f_{ZNM}(s) &= K_{ZN} \frac{1 - e^{-T_{ZN}s}}{T_{ZN}s} e^{-\tau_{ZN}s}, \\
 K_{AEFPI} &= \frac{1}{K_{ZN}} \left(\frac{T_{ZN}}{T_{ZN} + \tau_{ZN}} + 0.5 \right), \\
 T_{AEFTF} &= T_{ZN} + \tau_{ZN} - \frac{T_{EFTF}}{2}, \\
 T_{EFTF} &= \frac{1}{\omega_{PFB}} \approx \frac{T_{ZN}}{2}
 \end{aligned} \tag{16}$$

where $f_{ZNM}(s)$, K_{ZN} , T_{ZN} , and τ_{ZN} are the transfer function, gain, time constant, and pure lag constant of the ZNM [26], respectively.

The ZNM represents an engineering modeling of a process. Based on the previously given process, the process ZNM was created, as shown in Figure 20.

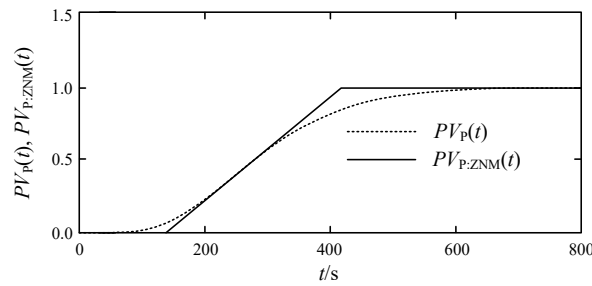


Figure 20. The procedure output from the ZNM.

$PV_P(t)$ and $PV_{P:ZNM}(t)$ represent the process outputs of the process and the process ZNM, respectively.

Based on Figure 20, the process ZNM was obtained as

$$\begin{aligned}
 f_{P:ZNM}(s) &= \frac{1-e^{-288s}}{288s} e^{-138s}, \\
 K_{ZNM} &= 1, \\
 T_{ZNM} &= 288s, \\
 \tau_{ZNM} &= 138s
 \end{aligned}
 \tag{17}$$

where $f_{P:ZNM}(s)$ is the transfer function of the process ZNM.

Based on Equations (16) and (17), $T_{AEFTF} = 354$ s, $K_{AEFTF} = 1.176$, and $T_{AEFTF} = 144$ s. The relationship between PM_{OLS} and AM_{OLS} with the variation in P_G and T_P was obtained, as shown in Figure 21.

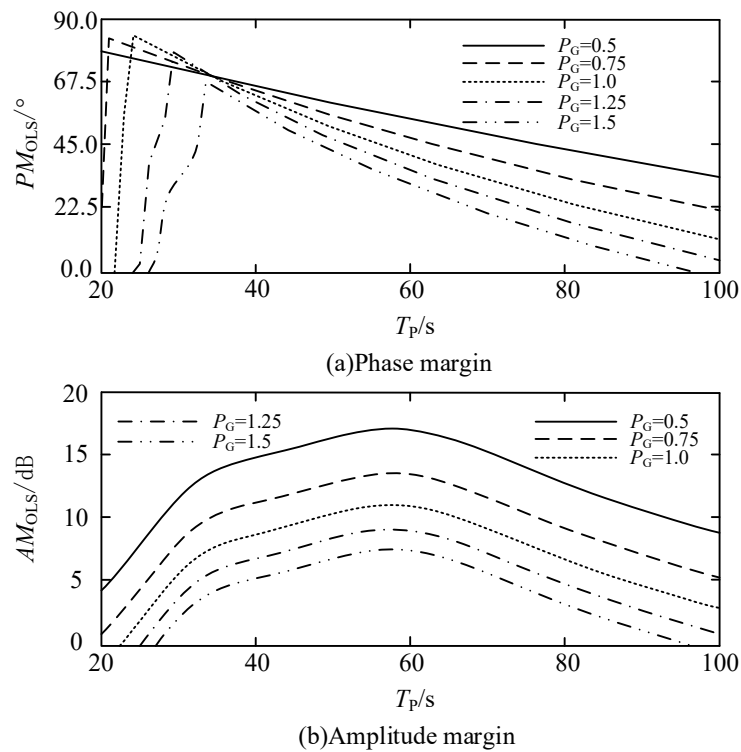


Figure 21. The result of the margin analysis is 3.

The simulated experimental results of the EFC were obtained, as shown in Figure 22.

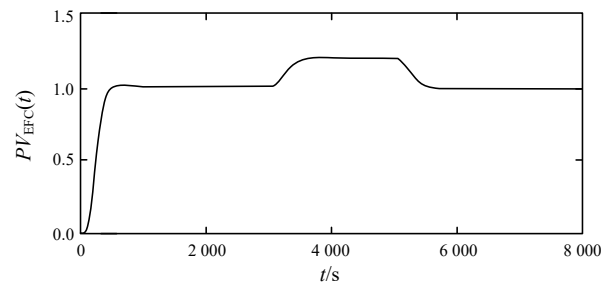


Figure 22. The simulation results of the EFC.

According to Figure 22, the regulation time of EFC control is 433.5 s, the overshoot of the process is 0.022, and the maximum deviation during the RF is 0.207. The engineering tuning of the EFC parameters has good performance and robustness.

6. Engineering Applications

The process control of thermal power units mainly adopts the strategy of open-loop control and feedback correction [27], the open-loop control relies on feedforward control [28], and the feedback correction is based on PID. From the point of view of feedback correction, the EFC significantly improves the feedback correction performance compared with PID.

In a 1000 MW ultra-supercritical thermal power unit, in order to realize the auxiliary frequency control, the EFC is used to optimize the systems of the main control of steam engines, main control of boilers, feedwater control [29], main steam temperature control [30], and the flue gas baffle control of the reheat steam temperature. The optimized structure of the boiler master control system is shown in Figure 23.

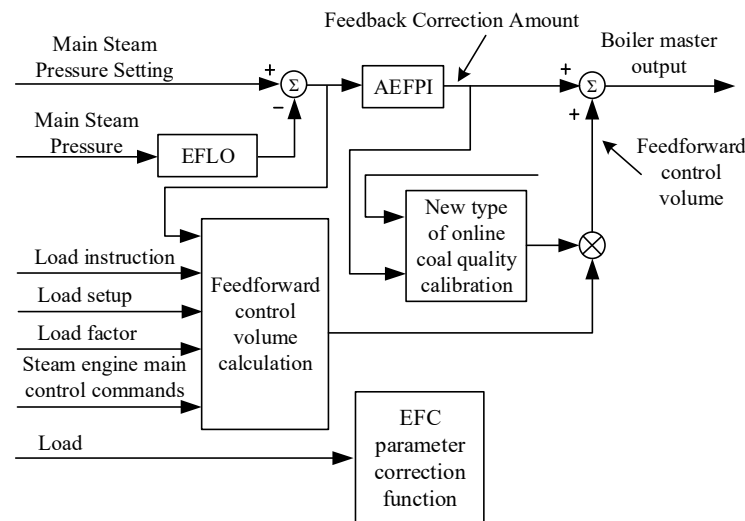


Figure 23. The optimization of the master control system of a boiler.

As illustrated in Figure 23, the feedforward control quantity calculation is used to calculate the feedforward control quantity according to the deviation in the main steam pressure from the main steam pressure given the load command, the load, the load rate, the main control command of the steam engine, etc. The new coal quality online correction is employed to facilitate the real-time adjustment of coal quality. The new coal quality online correction can assist power grid enterprise researchers in further meeting the needs of auxiliary frequency control and developing the basic principle according to the deviation in the feedback correction quantity. Through the adjustment of the feedforward control quantity, the feedback correction quantity for the long term can be determined, such as

the average value of 10 h to control in the vicinity of 0. Details of the new coal quality online correction can be found in Reference [27]. The EFC parameter correction function, which is used to modify the EFC parameters according to the load to ensure that the EFC parameters have good tracking characteristics for the unit load changes, is understood by engineering researchers as a form of “active adaptive control”.

With the unit load of 680 MW, through the field test, the approximate transfer function of the boiler master control object was obtained as

$$f_{P:680MW}(s) = \frac{0.93}{(1 + 79s)^6} \quad (18)$$

where $f_{P:680MW}(s)$ is the approximate transfer function of the controlled object at the unit load of 680 MW.

The 1 h operation trend of the system after commissioning is shown in Figure 24.

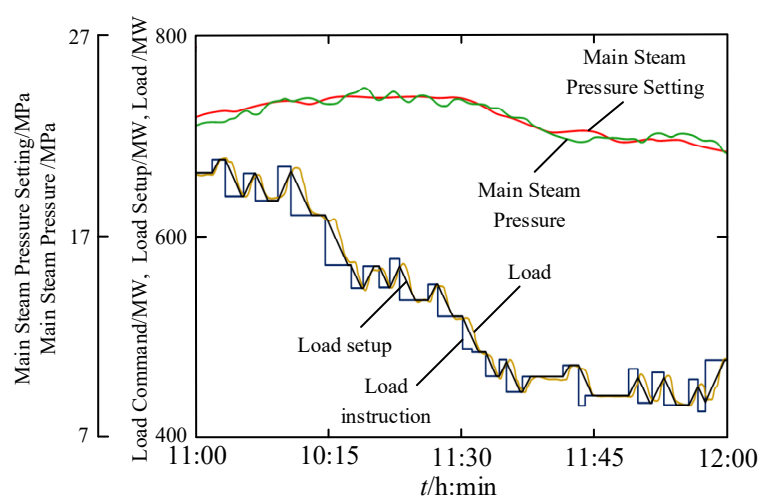


Figure 24. The control properties of the master control system of the boiler after optimization.

Figure 24 illustrates that in the auxiliary frequency control mode, the load command has obvious randomness in order to adapt to the new energy power load random change of regulation needs. In the given trend range, the range of load change is 430 MW–680 MW, the variable load rate is 20 MW/min, the maximum dynamic error between the load and load setting is 11 MW, and the absolute deviation between the main steam pressure and the main steam pressure setting is less than 0.56 MPa. The indexes of the load control and main steam pressure control satisfy the requirements of the relevant thermal power unit operation regulations.

7. Conclusions

The issue of control constraints in industrial environments is addressed, focusing on the limitations of the HGLO and HOC under NPG constraints, which is of some significance for the comprehensive understanding of the higher-order ahead observer and higher-order controller.

The EFC with an AEFPI and EFLO structure is investigated and experimented, and the theoretical basis for the significant breakthrough of the engineering fastest controller to the upper limits of the control performance of PI, PID, and SOC is given. The relative stability margin gives a reference for PI, PID, and SOC parameter optimization.

The engineering maximum speed controller is a mature new industrial control technology. There is a large number of engineering practices based on the “dual-carbon” energy target background from the point of view of the process control of the existing thermal

power units. Improving the controller's perturbation suppression performance is the main aspect of this research. The research and experimental results are of great practical significance and provide theoretical and technical guidance for the subsequent engineering of the maximum speed controller.

It should be noted that the theoretical issues behind engineering the fastest controllers are not problems that can be easily solved in a short period of time.

Author Contributions: Conceptualization, S.S. and J.L.; methodology, J.L.; software, S.S. and J.L.; validation, Y.H., R.L. and P.C.; formal analysis, Y.H.; writing—original draft preparation, S.S. and J.L.; writing—review and editing, Y.H. and P.C.; visualization, R.L.; project administration, S.S.; funding acquisition, P.C. All authors have read and agreed to the published version of the manuscript.

Funding: This research was funded by the Shanxi Province key research and development program (202202020101001).

Data Availability Statement: The data presented in this study are available on request from the corresponding author. The data are not publicly available due to privacy.

Conflicts of Interest: Author Jun Li was employed by the company Electric Power Research Institute of Guangdong Power Grid Co., Ltd. The remaining authors declare that the research was conducted in the absence of any commercial or financial relationships that could be construed as a potential conflict of interest.

Abbreviations

PID	proportional–integral–differential
CI	conventional integrator
FOIF	first-order inertial filter
EFTF	engineering fastest tracking filter
EFC	engineering fastest controller
SNR	signal noise ratio
NPG	noise power gain
PI	proportional–integral
HOC	high-order controller
HOLO	high-order leading observer
LO	leading observer
PD	proportional–differential
ATLO	A-type leading observer
BTLO	B-type leading observer
SOC	sixth-order controller
DM	disturbance model
RF	ramp function
RZFG	relative zero frequency gain
RSM	relative stability margin
EFLO	engineering fastest leading observer
AEFPI	accelerated engineering fastest proportional–integral
AEFTF	acceleration engineering fastest tracking filter
AFTF	acceleration fastest tracking filter
FTF	fastest tracking filter
SOF	second-order filter
ZNM	Ziegler–Nichols model

References

1. Ding, L.; Ding, Y.; Xing, X.; Zhu, J.; Zhang, W. Development Status, Challenges and Recommendations for Carbon Measurement in the context of emission peak and carbon neutrality goals. *Metrol. Meas. Tech.* **2024**, *50*, 11–15.
2. Liu, Y.; Peng, M.; Gao, X. Dynamic vulnerability assessment of hybrid system considering wind power uncertainty. *Energy Rep.* **2024**, *11*, 3721–3730. [[CrossRef](#)]
3. Liang, Y.; Li, P.; Su, W.; Li, W.; Xu, W. Development of green data center by configuring photovoltaic power generation and compressed air energy storage systems. *Energy* **2024**, *292*, 130516. [[CrossRef](#)]
4. Sugawara, D.; Saitoh, H.; Ito, N.; Kakeda, K. Fair Output Limit Determination Method of Wind Farms to Reduce Curtailed Power by Demand Response. *IEEE Trans. Electr. Electron. Eng.* **2023**, *18*, 1856–1868. [[CrossRef](#)]
5. Dellaly, M.; Skander-Mustapha, S.; Slama-Belkhodja, I. Optimization of a residential community's curtailed PV power to meet distribution grid load profile requirements. *Renew. Energy* **2023**, *218*, 119342. [[CrossRef](#)]
6. Zhou, J.; Zhang, L.; Zhu, L.; Zhang, W. A data-driven operating improvement method for the thermal power unit with frequent load changes. *Appl. Energy* **2024**, *354*, 122195. [[CrossRef](#)]
7. Mohindru, P. Review on PID, fuzzy and hybrid fuzzy PID controllers for controlling non-linear dynamic behaviour of chemical plants. *Artif. Intell. Rev.* **2024**, *57*, 97. [[CrossRef](#)]
8. Sakthivel, N.K.; Sutha, S. Single Stage Grid-Connected Flyback Inverter with Optimal PID Controller for Harmonic Distortion Analysis. *J. Electr. Eng. Technol.* **2023**, *18*, 2153–2168. [[CrossRef](#)]
9. Huang, L.; Peng, Z.; Wang, J. Control Science: Inspired by Applications. *Sci. Technol. Rev.* **2011**, *29*, 72–79.
10. Lin, J.; Huang, W.; Wan, W.; Liu, Z. Research and application of a novel feedback controller. *Control Theory Appl.* **2020**, *37*, 411–422.
11. Chen, X.; Zhu, X. Application of engineering maximum speed controller in ultra-supercritical secondary reheat unit. *Boil. Manuf.* **2023**, *5*, 18–20.
12. Zhang, D.; Chen, G.; Guo, G.; Wang, Y.; Lv, F.; Wang, Y.; Gao, S. Method of Multi-Energy Complementary System Participating in Auxiliary Frequency Regulation of Power Systems. *Electronics* **2024**, *13*, 906. [[CrossRef](#)]
13. Ranginkaman, S.; Mashhour, E.; Saniei, M. Bidding strategy of the virtual power plant consisting of thermal loads controlled by thermostats for providing primary frequency control ancillary service. *Sustain. Energy Grids Netw.* **2024**, *38*, 101242. [[CrossRef](#)]
14. Shi, S.; Chen, J.; Li, J.; Liu, J.; Wang, Z.; Li, Z.; Chen, P.; Li, L. Engineering Fastest Control: A New Process Control Method for Thermal Power Units. *Energies* **2024**, *17*, 924. [[CrossRef](#)]
15. Sun, X.; Peng, C.; Cheng, C. Transfer reinforcement learning control for a selective catalytic reduction denitration system under complex conditions. *Control Theory Technol.* **2024**, *41*, 496–501.
16. Cui, X.; Xu, P.; Song, G.; Gu, H.; Gu, H.; Wang, L.; Zhu, H. PID Control of a Superheated Steam Temperature System Based on Integral Gain Scheduling. *Energies* **2022**, *15*, 8978. [[CrossRef](#)]
17. Shi, S.; Li, J.; Liu, Z.; Liu, J.; Chen, P. A novel fastest control technology: Principles and applications. *Control Theory Appl.* **2024**, *41*, 1408–1416.
18. Abdo Jaoude, A. The paradigm of complex probability and Claude Shannon's information theory. *Syst. Sci. Control Eng.* **2017**, *5*, 380–425. [[CrossRef](#)]
19. Chen, H.; Chan, E.H.W. All-optical high-order subharmonic mixer with a high signal-to-noise ratio and stable performance. *Appl. Opt.* **2024**, *63*, 359–366. [[CrossRef](#)]
20. Shishter, Y.M.; Ali, F.H.; Young, R.C. Scintillation and bit error rate analysis of zero-order Bessel–Gauss beams in atmospheric turbulence based on the extended Rytov theory. *Opt. Eng.* **2024**, *63*, 041205. [[CrossRef](#)]
21. Wang, J.; Zhang, X.; Wang, X.; Yang, X. Global h-synchronization of stochastic delayed high-order inertial neural networks subject to Markovian jump parameters. *J. Frankl. Inst.* **2023**, *360*, 2848–2866. [[CrossRef](#)]
22. Hecq, A.; Laurent, S.; Palm, F.C. On the Univariate Representation of BEKK Models with Common Factors. *J. Time Ser. Econom.* **2016**, *8*, 91–113. [[CrossRef](#)]
23. Barradas, V.R.; Koike, Y.; Schweighofer, N. Theoretical limits on the speed of learning inverse models explain the rate of adaptation in arm reaching tasks. *Neural Netw.* **2024**, *170*, 376–389. [[CrossRef](#)] [[PubMed](#)]
24. Grebenshchikov, B.G.; Lozhnikov, A.B. Asymptotic Properties of a Class of Systems with Linear Delay. *Differ. Equ.* **2023**, *59*, 577–590. [[CrossRef](#)]
25. Sengar, K.; Kumar, A. Fractional Order Capacitor in First-Order and Second-Order Filter. *Micro Nanosyst.* **2020**, *12*, 75–78. [[CrossRef](#)]
26. Ziegler, J.G.; Nichols, N.B. Optimum settings for automatic controllers. *Trans. Am. Soc. Mech. Eng.* **1942**, *64*, 759–765. [[CrossRef](#)]
27. Chen, J.; Zhao, B.; Sun, W.; Luo, D.; Liao, F.; Wang, W.; Liang, X.; Wang, L.; Li, D. Mechanism Research and Application of the Accelerated Engineering Fastest Proportional-Integral Controller. *Control Instrum. Chem. Ind.* **2023**, *50*, 745–753+874.
28. Liu, B.; Song, Z.; Yu, B.; Yang, G.; Liu, J. A Feedforward Control-Based Power Decoupling Strategy for Grid-Forming Grid-Connected Inverters. *Energies* **2024**, *17*, 424. [[CrossRef](#)]

29. Tran, T.C.; Jung, J.C. Development of Anti-windup PI Control and Bumpless Control Transfer Methodology for Feedwater Control System. *Ann. Nucl. Energy* **2019**, *131*, 233–241. [[CrossRef](#)]
30. Lian, L. Main steam temperature control based on variable universe fuzzy dynamic matrix control. *Therm. Eng.* **2022**, *69*, 763–778. [[CrossRef](#)]

Disclaimer/Publisher’s Note: The statements, opinions and data contained in all publications are solely those of the individual author(s) and contributor(s) and not of MDPI and/or the editor(s). MDPI and/or the editor(s) disclaim responsibility for any injury to people or property resulting from any ideas, methods, instructions or products referred to in the content.